

**NUCLEAR STRUCTURE FUNCTIONS AND HEAVY FLAVOUR
LEPTOPRODUCTION OFF THE NUCLEUS AT SMALL x IN
PERTURBATIVE QCD**

N. Armesto

*Departamento de Física, Módulo C2, Planta baja, Campus de Rabanales,
Universidad de Córdoba, E-14071 Córdoba, Spain*

and

M. A. Braun¹

*Departamento de Física de Partículas, Universidade de Santiago de Compostela,
E-15706 Santiago de Compostela, Spain*

Abstract

Nuclear structure functions and cross-sections for heavy flavour production in lepton-nucleus collisions are investigated in the low x region accessible now or in the near future. The scattering on a heavy nucleus is described by the sum of fan diagrams of BFKL pomerons, which is exact in the high-colour limit. The initial condition for the evolution at $x = 0.01$ is taken from a saturation model, which reproduces the experimental data on the proton. The A dependence of the structure functions is well described by a power factor A^α , with α reaching values as low as $1/2$ at extremely low x . The total cross-sections for heavy flavour production reach values of the order of mb, and the corresponding transverse momentum distributions are sizeable up to transverse momenta larger than the initial large scale $\sqrt{Q^2 + 4m_f^2}$.

1 Introduction

In the framework of the colour dipole model [1,2] and in the high-colour limit $N_c \rightarrow \infty$, the scattering on a heavy nucleus is exactly described by the sum of fan diagrams constructed of BFKL pomerons, each of them splitting into two. Numerical solutions of the resulting equation for the colour dipole cross-section on the nucleus [3-9] were first presented in [8], and then in [10-14]. The gluon density introduced in [8] revealed a "supersaturation" behaviour, tending to zero at any fixed momentum k as the rapidity $Y \rightarrow \infty$. As a function of $\ln k$ it proved to have a form of a soliton wave moving to the right with a constant velocity as Y increases. This latter phenomenon is related to its scaling property: at high enough Y the gluon density at fixed impact parameter b proved to be a function of the ratio $k/Q_s(Y, b)$, where $Q_s(Y, b)$, the position in momentum space of the maximum of the gluon density, can be interpreted as a "saturation momentum" growing as a power of energy. Subsequent numerical calculations [10,14] confirmed this scaling behaviour, although the gluon density itself is defined differently by different authors.

Obviously partonic densities in the nucleus are not observable themselves but are only certain theoretical tools to calculate the observable quantities. Therefore different definitions

¹On leave of absence from Department of High-Energy Physics, St. Petersburg University, 198504 St. Petersburg, Russia.

of the gluonic density are well admissible, provided they lead to the same observables. As such the structure function of the nucleus is the most directly calculable one. It was first calculated in [8] from the found solution of the BFKL fan diagram equation for a very wide range of energies (up to rapidities ~ 50), for the nucleus in the form of a spherical well and for a rather specific colour distribution inside the nucleon, not adapted to the experimental data. The found structure function proved to be rising as Y with rapidity and roughly linearly with Q^2 in agreement with the theoretical expectations [7,11]. Later calculations with a more realistic nuclear density [15] revealed that the nuclear structure function in fact grows as Y^2 , the extra growth provided by the contribution of peripheral collisions not damped by the non-linear term in the evolution equation. Still the attention in both [8] and [15] was centered at the asymptotic behaviour at high energies, insensitive to the choice of the initial conditions and governed only by the internal dynamics of the evolution equation.

However, from the experimental point of view it is desirable to know the structure function at values of x accessible now or in the near future (see e.g. [16]), say down to 10^{-7} corresponding to $Y \leq 16 \div 17$. At such rapidities the influence of the initial condition is still rather noticeable so that its choice becomes a matter of importance. Accordingly we performed a new run of calculations employing more realistic colour distributions in the proton, following from the saturation approach of [17] consistent with DIS data for the proton below $x = 0.01^2$. In [10] the parton distributions following from this initial condition were studied. In this paper we report on the nuclear structure function following from the BFKL fan diagram evolution equation with physically supported initial conditions. The solution of this equation also allows us to find the gluon density in the nucleus. We use it to study another directly measurable quantity: the inclusive probability for heavy flavour production off nuclei (by photon-gluon fusion) in photon induced reactions.

2 The nuclear structure function from the evolution equation

In this section we collect the formulae necessary to calculate the structure function from the solution of the BFKL fan diagram evolution equation. The nuclear structure function F_2 can be standardly defined via the cross-sections $\sigma_{T,L}$ for the collision of the transversal (T) or longitudinal (L) virtual photon of momentum q , $q^2 = -Q^2$, on the nucleus A of momentum Ap :

$$F_2(x, Q^2) = \frac{Q^2}{\pi e^2} (\sigma_T + \sigma_L), \quad (1)$$

where $x = \exp(-Y) = Q^2/(2q \cdot p)$. Both cross-sections can be conveniently presented via the cross-section $\sigma_{dA}(Y, r)$ for the scattering of a colour dipole of the transverse radius r on the nucleus:

$$\sigma_{T,L}(Y) = \int d^2r \rho_{T,L}(r) \sigma_{dA}(Y, r), \quad (2)$$

where $\rho_{T,L}$ is a well-known distribution of colour dipoles created by splitting of the incident photon into $q\bar{q}$ pairs:

$$\rho_T(r) = \frac{e^2 N_c}{8\pi^3} \sum_f Z_f^2 \int_0^1 d\alpha \left\{ [\alpha^2 + (1-\alpha)^2] \epsilon^2 K_1^2(\epsilon r) + m_f^2 K_0^2(\epsilon r) \right\} \quad (3)$$

²Other approaches [18] which explicitly contain saturation in the form of multiple scattering and also describe the experimental data for the proton, could be used, see [19] for a study of saturation in the low Q^2 region within this multiple scattering model. We will restrict ourselves to the use of [17] due to technical reasons, see Section 3.

and

$$\rho_L(r) = \frac{e^2 N_c}{2\pi^3} Q^2 \sum_f Z_f^2 \int_0^1 d\alpha \alpha^2 (1-\alpha)^2 K_0^2(\epsilon r). \quad (4)$$

Here summation goes over flavours, $\epsilon^2 = Q^2 \alpha(1-\alpha) + m_f^2$, and m_f and Z_f are respectively the mass and electric charge in units of e , of the quark of flavour f .

The dipole-nucleus cross-section in its turn can be presented as an integral over the impact parameter b :

$$\sigma_{dA}(Y, r) = 2 \int d^2b \Phi(Y, r, b), \quad (5)$$

where 2Φ has a meaning of the cross-section at fixed impact parameter. The evolution equation in Y can be most conveniently written for the function

$$\phi(Y, r, b) = \frac{1}{2\pi r^2} \Phi(Y, r, b) \quad (6)$$

in momentum space. It reads [8]

$$\left(\frac{\partial}{\partial y} + H_{BFKL} \right) \phi(y, q, b) = -\phi^2(y, q, b), \quad (7)$$

where $y = \alpha_s N_c Y / \pi$ and H_{BFKL} is the forward BFKL Hamiltonian.

Putting (6) into (5) and (2), and passing to the momentum space, we can express the cross-sections $\sigma_{T,L}$ directly via the function ϕ or its 2nd derivative in the logarithm of the momentum:

$$\sigma_{T,L} = \frac{1}{\pi} \int d^2b d^2q \phi(y, q, b) w_{T,L}(q) = \frac{1}{\pi} \int d^2b \frac{d^2q}{q^2} h(y, q, b) \tilde{\rho}_{T,L}(q), \quad (8)$$

where

$$\tilde{\rho}_{T,L}(q) = \int d^2r \rho_{T,L}(r) (1 - e^{i\mathbf{q}\mathbf{r}}), \quad w_{T,L}(q) = \int d^2r r^2 \rho_{T,L}(r) e^{i\mathbf{q}\mathbf{r}} \quad (9)$$

and

$$h(y, q, b) = q^2 \nabla_q^2 \phi(y, q, b) = \frac{\partial^2 \phi(y, q, b)}{(\partial \ln q)^2}. \quad (10)$$

Up to a trivial factor, function h gives the gluon density in the nucleus [8]:

$$\frac{\partial x G(x, k^2, b)}{\partial^2 b \partial k^2} = \frac{2N_c}{\pi g^2} k^2 \nabla_k^2 \phi \left(\ln \frac{1}{x}, k, b \right). \quad (11)$$

This definition is not unique (see the discussion in [20]) but natural in the sense that the structure function can be directly expressed via the gluon density thus defined. We shall see later that this is also true for other observables.

Note that for numerical calculations the first form in (8) is much more convenient, since it requires neither numerical differentiation nor taking into account the singularity at $q = 0$. Functions $w_{T,L}$ can be easily found analytically:

$$w_T(q) = \frac{e^2 N_c}{8\pi^2} \nabla_q^2 \sum_f Z_f^2 \int_0^1 d\alpha \left[(\alpha^2 + (1-\alpha)^2) (q^2/2 + \epsilon^2) - m_f^2 \right] J(q, \epsilon), \quad (12)$$

where

$$J(q, \epsilon) = \frac{2}{q \sqrt{q^2 + 4\epsilon^2}} \ln \frac{\sqrt{q^2 + 4\epsilon^2} + q}{\sqrt{q^2 + 4\epsilon^2} - q}. \quad (13)$$

The longitudinal density w_L is given by the same expression without the term with m_f^2 and with the substitutions

$$\alpha^2 + (1 - \alpha)^2 \rightarrow \alpha(1 - \alpha), \quad q^2/2 + \epsilon^2 \rightarrow -4\epsilon^2.$$

Formulae (8)-(13) allow to find the nuclear structure function provided function ϕ is known from the evolution equation (7). To solve the latter one should fix the initial conditions for the evolution, that is, the $\phi(y, q, b)$ at the starting point of the evolution which we denote as $y = 0$.

3 Initial conditions for the evolution

The initial function $\phi_0(q, b) = \phi(y = 0, q, b)$ can be expressed via the dipole-nucleus cross-section at $y = 0$ and fixed b :

$$\phi_0(q, b) = \int \frac{d^2r}{2\pi r^2} e^{i\mathbf{q}\mathbf{r}} \Phi_0(r, b) = \int_0^\infty \frac{dr}{r} J_0(qr) \Phi_0(r, b), \quad (14)$$

where $\Phi_0(r, b) = \Phi(Y = 0, r, b)$.

Staying in the BFKL picture, with a fixed small strong coupling constant α_s , at $Y = 0$ the scattering of a dipole on the nucleus is described by the Glauber formula with the dipole-nucleon cross-section $\sigma(r)$ given by the two-gluon exchange:

$$\Phi_0(r, b) = 1 - e^{-\frac{1}{2}AT(b)\sigma(r)}. \quad (15)$$

Here

$$\sigma(r) = g^4 \int d^2r' G(0, r, r') \rho_p(r'), \quad (16)$$

$\rho_p(r)$ is the colour dipole density in the proton and $G(0, r, r')$ is the BFKL Green function at $Y = 0$:

$$G(0, r, r') = \frac{rr'}{8\pi} \frac{r_{<}}{r_{>}} \left(1 + \ln \frac{r_{>}}{r_{<}} \right), \quad r_{>(<)} = \max(\min)\{r, r'\}. \quad (17)$$

$T(b)$ is the nuclear profile function normalized to 1. Obviously the density ρ_p is non-perturbative and not known. If, as in [8], to simplify the calculations one chooses ρ_p to be a Yukawa distribution

$$\rho_p(r) = a \frac{e^{-\mu r}}{r}, \quad (18)$$

then one obtains

$$\frac{1}{2}AT(b)\sigma(r) = B \left[2C - 1 + 2 \ln \tilde{r} - \text{Ei}(-\tilde{r}) \left(2 + \tilde{r}^2 \right) + e^{-\tilde{r}}(1 - \tilde{r}) \right], \quad \tilde{r} = \mu r, \quad (19)$$

where C is the Euler constant and dimensionless B combines the information about the nucleus density, value of α_s and normalization constant a in (18). At $r \rightarrow 0$ and ∞ , (19) behaves as $r^2 \ln(1/r)$ and $\ln r$ respectively.

However this sort of initial conditions is only true in the rigorous BFKL approach with a fixed and very small coupling. In fact, if one calculates the structure function of the proton using (19), one finds a very strong Q^2 dependence incompatible with the experimental data. To be nearer the realistic situation we therefore choose the dipole-nucleon cross-section $\sigma(r)$ in (15) to be in agreement with the DIS data at moderately low x , at which one may expect the start of the evolution according to Eq. (7). We take $x = 0.01$ as a starting point for the

evolution and choose $\sigma(r)$ as parametrized by Golec-Biernat and Wüsthoff [17] to reproduce all DIS data on the proton below $x = 0.01$:

$$\sigma(r) = \sigma_0 \left(1 - e^{-\hat{r}^2}\right), \quad \hat{r} = \beta r, \quad (20)$$

with $\sigma_0 = 29.12$ mb and $\beta = 0.234$ GeV for 4 quark flavours (with masses $m_u = m_d = m_s = 0.14$ GeV and $m_c = 1.5$ GeV, which we will use in all our computations). Nevertheless, these values have been obtained from a fit to experimental data with $x \leq 0.01$ and we are interested only in $\sigma(r)$ at $x = 0.01$, where the quoted values produce a cross-section which overestimates the experimental data for F_2 of the proton, while the Q^2 evolution at this x is well described. Thus, to better agree with the experimental data at $x = 0.01$ we diminished σ_0 to a lower value 20.80 mb, keeping the value of β ; we have verified that with this choice, Eq. (15) reasonably reproduces F_2 in nuclei at this value of x , see e.g. [21] for another use of (15) in this context. Apart from being in agreement with the experimental data, the cross-section (20) has an advantage of allowing to relatively simply Bessel transform the Glauberized cross-section (15) to obtain the initial function ϕ in the momentum space according to (14) (see Appendix).

4 Heavy flavour production off the nucleus

The total cross-section for the photoproduction of heavy flavour f off the nucleus is given by σ_T at $Q^2 = 0$ with w_T corresponding to the contribution of this flavour in the sum (12). The inclusive cross-section for the production of the heavy quark with a given transverse momentum l can be obtained from the expression for the heavy quark density (see [10,22]):

$$\begin{aligned} \frac{\partial[xq_f(x, l, b)]}{\partial^2 l \partial^2 b} &= \frac{\alpha_s Q^2}{(2\pi)^3} \int_0^1 d\alpha d^2 b_1 d^2 b_2 e^{-i l(\mathbf{b}_1 - \mathbf{b}_2)} \\ &\left[\left(\alpha^2 + (1 - \alpha)^2 \right) \epsilon^2 \frac{\mathbf{b}_1 \mathbf{b}_2}{b_1 b_2} K_1(\epsilon b_1) K_1(\epsilon b_2) + \left[4Q^2 \alpha^2 (1 - \alpha)^2 + m_f^2 \right] K_0(\epsilon b_1) K_0(\epsilon b_2) \right] \\ &\int \frac{d^2 k}{(2\pi)^2} \frac{1}{k^2} \frac{\partial[xG(x, k, b)]}{\partial^2 b \partial k^2} \left[1 + e^{-i k(\mathbf{b}_1 - \mathbf{b}_2)} - e^{-i k \mathbf{b}_1} - e^{i k \mathbf{b}_2} \right]. \end{aligned} \quad (21)$$

Note that, using (6) and (11) and the fact that $\Phi(Y, 0, b) = 0$, the last line of Eq. (21) can be rewritten as

$$\frac{N_c}{\pi^2 g^2} \left[\Phi(Y, \mathbf{b}_1, b) + \Phi(Y, \mathbf{b}_2, b) - \Phi(Y, \mathbf{b}_1 - \mathbf{b}_2, b) \right];$$

if we neglect the evolution in Y and take into account only the multiple Glauber rescattering in the nucleus implied by (15), we recover the result for the quark density in [22] (Eq. (26) in this reference). The inclusive cross-section is expressed via the density (21) as

$$\frac{d\sigma_f}{d^2 l} = \frac{4\pi^2 \alpha_{em}}{Q^2} Z_f^2 \int d^2 b \frac{\partial[xq_f(x, l, b)]}{\partial^2 l \partial^2 b}. \quad (22)$$

Evidently it is finite at $Q^2 = 0$ with only the transverse part surviving in this limit.

The leptoproduction cross-sections can be found once the cross-sections for the virtual photoproduction are known, which correspond to (21) and (22) at non-zero Q^2 :

$$\frac{d\sigma_f(e + A \rightarrow e' + Q + X)}{d^2 l dQ^2 dz} = \frac{\alpha_{em}}{\pi z Q^2} \left(1 - z + \frac{1}{2} z^2 \right) \frac{d\sigma_f(\gamma^* + A \rightarrow Q + X)}{d^2 l} \quad (23)$$

(see [23] for a discussion on the validity of the equivalent photon approximation in this kind of computations). Here z is the fraction of the energy of the incident electron carried by the

virtual photon: $z = q \cdot p / (p_l \cdot p)$, where Ap is the momentum of the nucleus and p_l that of the lepton.

It is remarkable that both total and inclusive cross-sections for the heavy flavour production are directly expressed via the gluon density (11) in our definition. This perfectly fits the assumed photon-gluon fusion production mechanism and thus supports our definition of the gluon density from a pragmatic point of view.

Performing part of the integrations and using Eqs. (10) and (11), we express the quark density as

$$\frac{\partial[xq_f(x, l, b)]}{\partial^2 l \partial^2 b} = \frac{Q^2 N_c}{8\pi^4} \int_0^\infty \frac{dk}{k} h(y, k, b) \int_0^1 d\alpha \left\{ \left[\alpha^2 + (1 - \alpha)^2 \right] I_T(\epsilon, k) + \left[4Q^2 \alpha^2 (1 - \alpha)^2 + m_f^2 \right] I_L(\epsilon, k) \right\}, \quad (24)$$

where function h is defined by (10),

$$I_T = \left(2\epsilon^2 + k^2 \right) \chi \xi - \epsilon^2 \left(\epsilon^2 + l^2 + k^2 \right) \chi^3 - \epsilon^2 \xi^2 \quad (25)$$

and

$$I_L = \left(\epsilon^2 + l^2 + k^2 \right) \chi^3 + \xi^2 - 2\chi \xi, \quad (26)$$

with

$$\xi = \frac{1}{\epsilon^2 + l^2}, \quad \chi = \frac{1}{\sqrt{(\epsilon^2 + (l + k)^2)(\epsilon^2 + (l - k)^2)}}. \quad (27)$$

These formulae allow to calculate the quark density both at $Q^2 = 0$ and at finite Q^2 once the gluon density in the nucleus (i.e. function h up to a numerical factor) is known from the solution of the evolution equation (7).

5 Numerical results

Starting from the initial function ϕ_0 at $x = 0.01$ described in Section 3 we solved numerically the evolution equation (7) for values of y up to $y_{max} = y_0 + 4.0$, where y_0 is the initial value of y . We have taken $\alpha_s = 0.2$, so that $y_0 \simeq 0.88$ and the minimal value of x is $\sim 10^{-11}$. For the nuclear profile function we use the one corresponding to the nuclear density given by a 3-parameter Fermi distribution, with the values of the parameters taken from [24]. We have taken into account the contribution of charm but neglected that of bottom, which is relatively small in the total structure function. The structure function of Pb in this interval of x and for different values of Q^2 between 10 and 10^5 (GeV/c)² is shown in Fig. 1. One observes that it grows roughly as $\ln^2(1/x)$ with x , and as Q^2 with Q^2 . Its A -dependence can be well represented by a power behaviour

$$F_{2A}(x, Q^2) = A^{\alpha(x, Q^2)} F(x, Q^2). \quad (28)$$

Power α results dependent both on x and Q^2 . It is presented in Fig. 2. One observes that at relatively large values of x α is close to unity and depends on Q^2 very weakly. However at smaller x the power goes down up to values below $2/3$ naively expected from the nuclear screening. At a given x it rises with increasing Q^2 , however the general trend of going down with $1/x$ persists at all Q^2 .

Our results for the total cross-section for the real and virtual photoproduction of charm and bottom (with $m_b = 4.75$ GeV) on various nuclei are presented in Figs. 3 and 4. The cross-sections are shown as functions of the photon c.m. energy W with respect to a nucleon in the nucleus. We assumed that

$$x = \frac{4m_f^2 + Q^2}{W^2 + Q^2}. \quad (29)$$

The minimal value of W corresponds to the maximal value of $x = 0.01$ for our solution. Accordingly it rises with Q^2 , which explains why the curves for different Q^2 start from different W . As expected, the cross-sections rise with increasing W and $1/Q^2$. Their absolute values are rather big, reaching ~ 3 and ~ 1 mb for charm and bottom respectively for Pb at $W = 1000$ GeV and $Q^2 = 0$. The growth with W in the shown interval $W < 10^4$ GeV is rather close to power-like. However, corresponding to the behaviour of the structure function (Fig. 1), at higher W this should change to $\sim \ln^2 W$.

In Figs. 5 and 6 we show the transverse momentum distribution of the produced charmed quark off Pb at $Q^2 = 0$ and 30 (GeV/c)² respectively, and at $W = 200, 1000$ and 5000 GeV (in mb/(GeV/c)²). Here we assumed that

$$x = \frac{4m_f^2 + Q^2 + 4l^2}{W^2 + Q^2}. \quad (30)$$

Our restriction $x < 0.01$, combined with discrete values of y at which the gluon density was calculated, severely limited the number of points at small W . This explains a somewhat irregular form of the curves at $W = 200$ GeV. One observes that, in accordance with the BFKL kinematics, a relatively large part of the charmed quarks are produced with momenta of the order or even larger than the initial large scale $\sqrt{Q^2 + 4m_f^2}$.

6 Discussion

We have calculated the nuclear structure functions at low x which follow from the fan diagram evolution equation in the perturbative QCD, with the initial conditions adjusted to the existing experimental data on DIS on the proton at $x = 0.01$. Knowing the gluon density in the nucleus we also calculated the total and inclusive cross-sections for charm and bottom production at low x . The results show that the structure functions grow with increasing $1/x$ and Q^2 as $\ln^2(1/x)$ and Q^2 respectively. Parametrizing the A dependence as A^α we found that at very small x , α is going down to values below $1/2$. The found transverse distributions of heavy quarks exhibit a relatively large contribution from the momenta comparable or even larger than the natural scale $\sqrt{4m_f^2 + Q^2}$.

Our results have been obtained in the pure BFKL kinematical regime without any additional cuts. However they are based on the approximation of large N_c . Therefore one should not expect that they remain valid at extremely small x when the $1/N_c^2$ corrections growing with $1/x$ may change the found behaviour.

We can compare our results for the structure functions with the recently obtained in [12]. Although the general trend is similar, our structure functions grow with $1/x$ considerably faster. In particular, for Au at $Q^2 = 100$ (GeV/c)² and $x = 10^{-7}$, and also taking $\alpha_s = 0.25$ as in [12], we obtain $F_{2A}/A \sim 140$ as compared to ~ 20 in [12]. The difference may come partly from a different initial condition, which in [12] was taken in a simplified form (with $\sigma(r)$ roughly proportional to r^2) and partly from the fact that in [12] the asymptotical form for the photon dipole distributions (3) and (4) at large Qr was used. The latter approximation seems of dubious validity to us, since in fact values $Qr \sim 1$ give the bulk of the contribution to the structure function. Besides, in [12] the integration over the dipole dimension r was cut at both small and large values, which obviously introduced a dependence on the cut-off parameters.

Acknowledgments

M. A. B. acknowledges financial support by Secretaría de Estado de Educación y Universidades of Spain, and also by a grant of RFFI of Russia. N. A. acknowledges financial support by CICYT of Spain under contract AEN99-0589-C02, and by Universidad de Córdoba. The authors are thankful to Profs. C. Merino, C. Pajares and G. Parente for attention to this work and helpful discussions.

7 Appendix. The initial function with the Golec-Biernat-Wüsthoff dipole cross-section

Using Eqs. (14), (15) and (20) and passing to the integration over $x = \beta r$ we write the initial function $\phi_0(q, b)$ as an integral

$$\phi_0(q, b) = \int_0^\infty \frac{dx}{x} J_0(qx/\beta) \left(1 - e^{-B[1-e^{-x^2}]} \right). \quad (31)$$

The dependence on b is contained in the dimensionless factor B :

$$B = \frac{1}{2} AT(b) \sigma_0. \quad (32)$$

In the following this dependence will be suppressed. We will also denote $z = q/\beta$.

We present the exponential as a power series in its argument:

$$1 - e^{-B[1-e^{-x^2}]} = - \sum_{n=1}^{\infty} \frac{(-B)^n}{n!} (1 - e^{-x^2})^n, \quad (33)$$

so that

$$\phi_0(q) = - \sum_{n=1}^{\infty} \frac{(-B)^n}{n!} I_n(z), \quad (34)$$

where

$$I_n(z) = \int_0^\infty \frac{dx}{x} J_0(xz) (1 - e^{-x^2})^n. \quad (35)$$

The integral I_n can be presented as

$$I_n(z) = \sum_{k=0}^n C_n^k (-1)^k \int_0^\infty \frac{dx}{x} J_0(xz) e^{-kx^2} = - \sum_{k=0}^n C_n^k (-1)^k \int_0^\infty \frac{dx}{x} J_0(xz) (1 - e^{-kx^2}). \quad (36)$$

The last integral in x can be found analytically. Indeed one has (see [25])

$$\int_0^\infty dx x^\mu e^{-\alpha x^2} J_\nu(zx) = \frac{z^\nu \Gamma((\mu + \nu + 1)/2)}{2^{\nu+1} \alpha^{(\mu+\nu+1)/2} \Gamma(\nu + 1)} {}_1F_1 \left(\frac{\mu + \nu + 1}{2}; \nu + 1; -\frac{z^2}{4\alpha} \right). \quad (37)$$

Taking $\nu = 0$ one has

$$\int_0^\infty dx x^\mu e^{-\alpha x^2} J_0(zx) = \frac{\Gamma((\mu + 1)/2)}{2\alpha^{(\mu+1)/2}} {}_1F_1 \left(\frac{\mu + 1}{2}; 1; -\frac{z^2}{4\alpha} \right). \quad (38)$$

We take the difference of two integrals (38) with different α 's,

$$\int_0^\infty dx x^\mu (e^{-\gamma x^2} - e^{-\alpha x^2}) J_0(zx) =$$

$$\frac{1}{2}\Gamma((\mu+1)/2)\left[\gamma^{-(\mu+1)/2}{}_1F_1\left(\frac{\mu+1}{2};1;-\frac{z^2}{4\gamma}\right)-\alpha^{-(\mu+1)/2}{}_1F_1\left(\frac{\mu+1}{2};1;-\frac{z^2}{4\alpha}\right)\right]. \quad (39)$$

The result is obviously finite at $\mu = -1$. To find it we put

$$\mu+1=2\Delta\rightarrow 0. \quad (40)$$

In this limit,

$$\gamma^{-\Delta}\simeq 1-\Delta\ln\gamma, \quad \alpha^{-\Delta}\simeq 1-\Delta\ln\alpha, \quad \Gamma(\Delta)\simeq 1/\Delta \quad (41)$$

and

$${}_1F_1(\Delta;1;t)\simeq 1+\Delta(\text{Ei}(t)-C-\ln(-t)), \quad t<0. \quad (42)$$

Putting this into (39) we find, in the limit $\Delta\rightarrow 0$,

$$\int_0^\infty\frac{dx}{x}\left(e^{-\gamma x^2}-e^{-\alpha x^2}\right)J_0(zx)=\frac{1}{2}\left[\text{Ei}\left(-\frac{z^2}{4\gamma}\right)-\text{Ei}\left(-\frac{z^2}{4\alpha}\right)\right]. \quad (43)$$

Taking here $\gamma\rightarrow 0$ we find the desired integral:

$$\int_0^\infty\frac{dx}{x}\left(1-e^{-\alpha x^2}\right)J_0(zx)=-\frac{1}{2}\text{Ei}\left(-\frac{z^2}{4\alpha}\right). \quad (44)$$

With the help of this formula one can find the integrals $I_n(z)$ as a finite sum of exponential integrals of different arguments, Eq. (36). Putting this into (34) gives the initial function ϕ_0 . For realistic values of the parameter $B\leq 3$ the convergence of the series in n is very fast, so that ϕ_0 can be calculated with very high accuracy at all q .

References

- [1] A. H. Mueller, Nucl. Phys. **B415** (1994) 373; A. H. Mueller and B. Patel, Nucl. Phys. **B425** (1994) 471.
- [2] N. N. Nikolaev and B. G. Zakharov, Z. Phys. **C64** (1994) 631.
- [3] L. V. Gribov, E. M. Levin and M. G. Ryskin, Phys. Rept. **100** (1983) 1.
- [4] A. H. Mueller and J. Qiu, Nucl. Phys. **B268** (1986) 427.
- [5] A. L. Ayala Filho, M. B. Gay Ducati and E. M. Levin, Nucl. Phys. **B493** (1997) 305.
- [6] I. I. Balitsky, hep-ph/9706411; Nucl. Phys. **B463** (1996) 99.
- [7] Yu. V. Kovchegov, Phys. Rev. **D60** (1999) 034008; **D61** (2000) 074018.
- [8] M. A. Braun, Eur. Phys. J. **C16** (2000) 337.
- [9] E. Iancu, A. Leonidov and L. McLerran, hep-ph/0011241; Phys. Lett. **B510** (2001) 133; E. Iancu and L. McLerran, Phys. Lett. **B510** (2001) 145.
- [10] N. Armesto and M. A. Braun, Eur. Phys. J. **C20** (2001) 517.
- [11] E. M. Levin and K. Tuchin, Nucl. Phys. **B573** (2000) 833; hep-ph/0101275.
- [12] E. M. Levin and M. Lublinsky, hep-ph/0104108.
- [13] M. A. Kimber, J. Kwieciński and A. D. Martin, Phys. Lett. **B508** (2001) 58.
- [14] M. Lublinsky, hep-ph/0106112.
- [15] M. A. Braun, hep-ph/0101070.
- [16] H. Abramowicz *et al.*, *TESLA Technical Design Report, Part VI, Chapter 2*, Eds. R. Klanner, U. Katz, M. Klein and A. Levy.
- [17] K. Golec-Biernat and M. Wüsthoff, Phys. Rev. **D59** (1999) 014017; **D60** (1999) 114023.
- [18] A. Capella, E. G. Ferreira, A. B. Kaidalov and C. A. Salgado, Nucl. Phys. **B593** (2001) 336; Phys. Rev. **D63** (2001) 054010.

- [19] N. Armesto and C. A. Salgado, hep-ph/0011352.
- [20] M. A. Braun, hep-ph/0010041.
- [21] N. Armesto and M. A. Braun, Z. Phys. **C75** (1997) 709.
- [22] A. H. Mueller, Nucl. Phys. **B558** (1999) 285.
- [23] S. Frixione, M. L. Mangano, P. Nason and G. Ridolfi, Phys. Lett. **B319** (1993) 339.
- [24] C. W. De Jager, H. De Vries and C. De Vries, Atom. Data Nucl. Data Tabl. **14** (1974) 479.
- [25] I. S. Gradshteyn and I. M. Ryzhik, *Table of Integrals, Series and Products*, Academic Press 1994.

Figure captions

Fig. 1: The structure function F_2 of Pb as a function of x at different Q^2 .

Fig. 2: The power α of the A -dependence of the nuclear structure functions as a function of x at different Q^2 .

Fig. 3: The total cross-sections for real and virtual photoproduction of charm on Pb (lower right plot), Ag (lower left plot), Cu (upper right plot) and Ne (upper left plot).

Fig. 4: The total cross-sections for real and virtual photoproduction of bottom on Pb (lower right plot), Ag (lower left plot), Cu (upper right plot) and Ne (upper left plot).

Fig. 5: The inclusive cross-section $d\sigma/d^2l$ for the real photoproduction of charmed quarks on Pb, as a function of the photon-nucleon c.m. energy W .

Fig. 6: The inclusive cross-section $d\sigma/d^2l$ for the virtual photoproduction at $Q^2 = 30$ (GeV/c)² of charmed quarks on Pb, as a function of the photon-nucleon c.m. energy W .

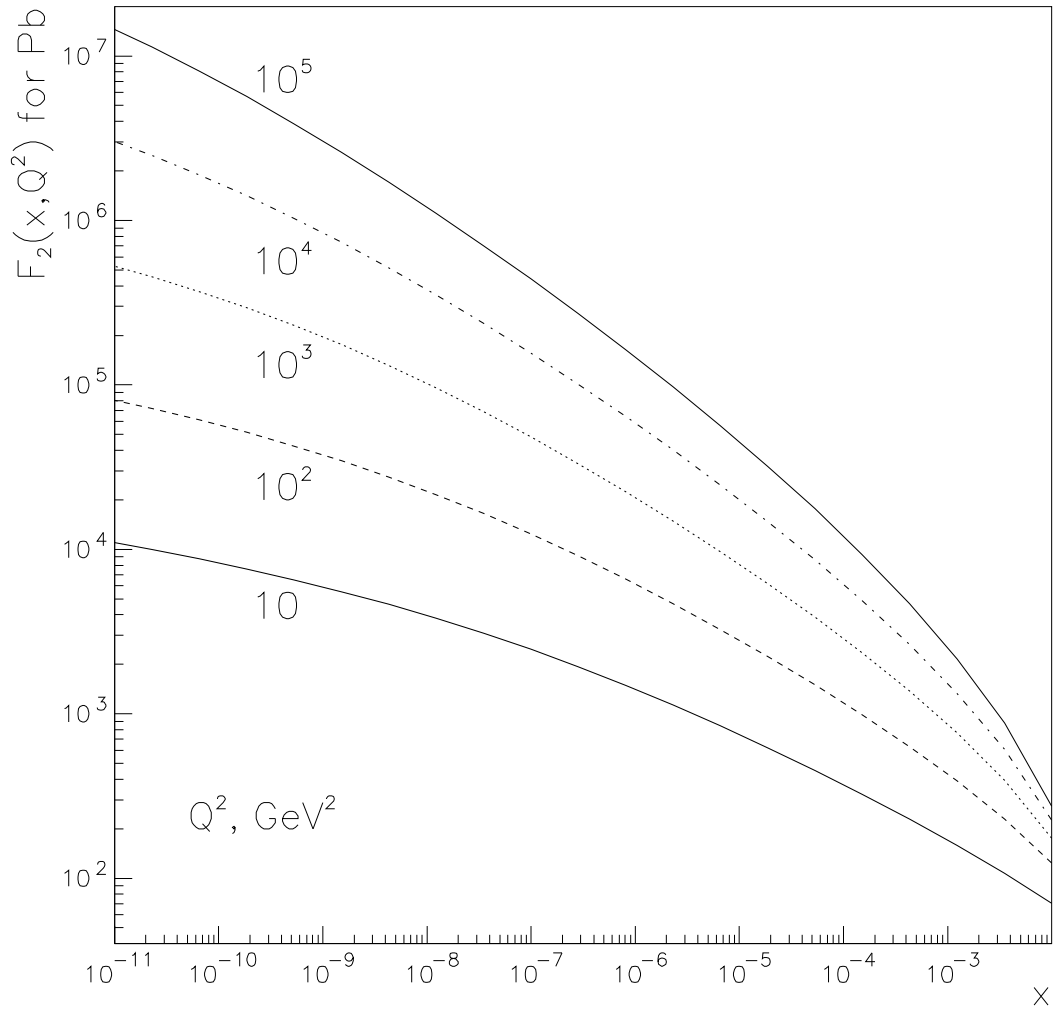


Figure 1:

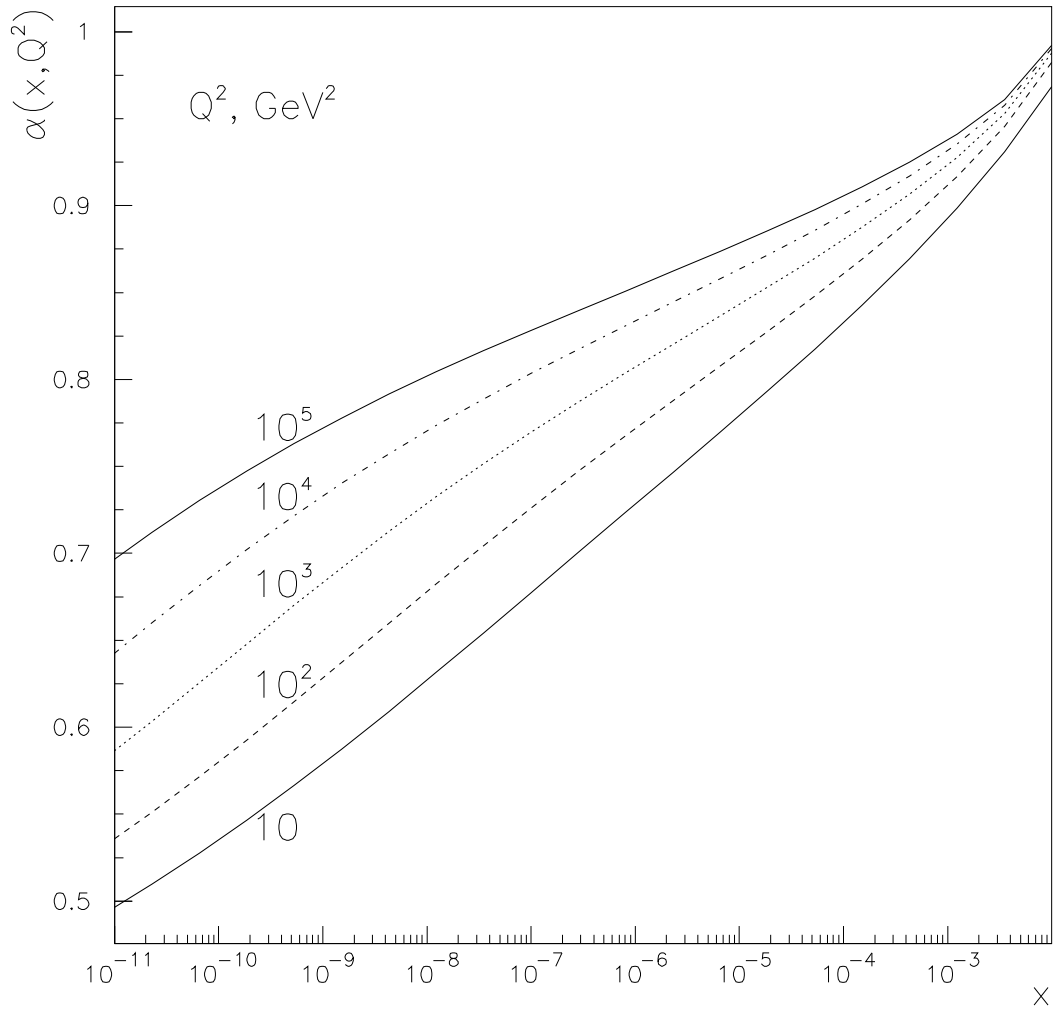


Figure 2:

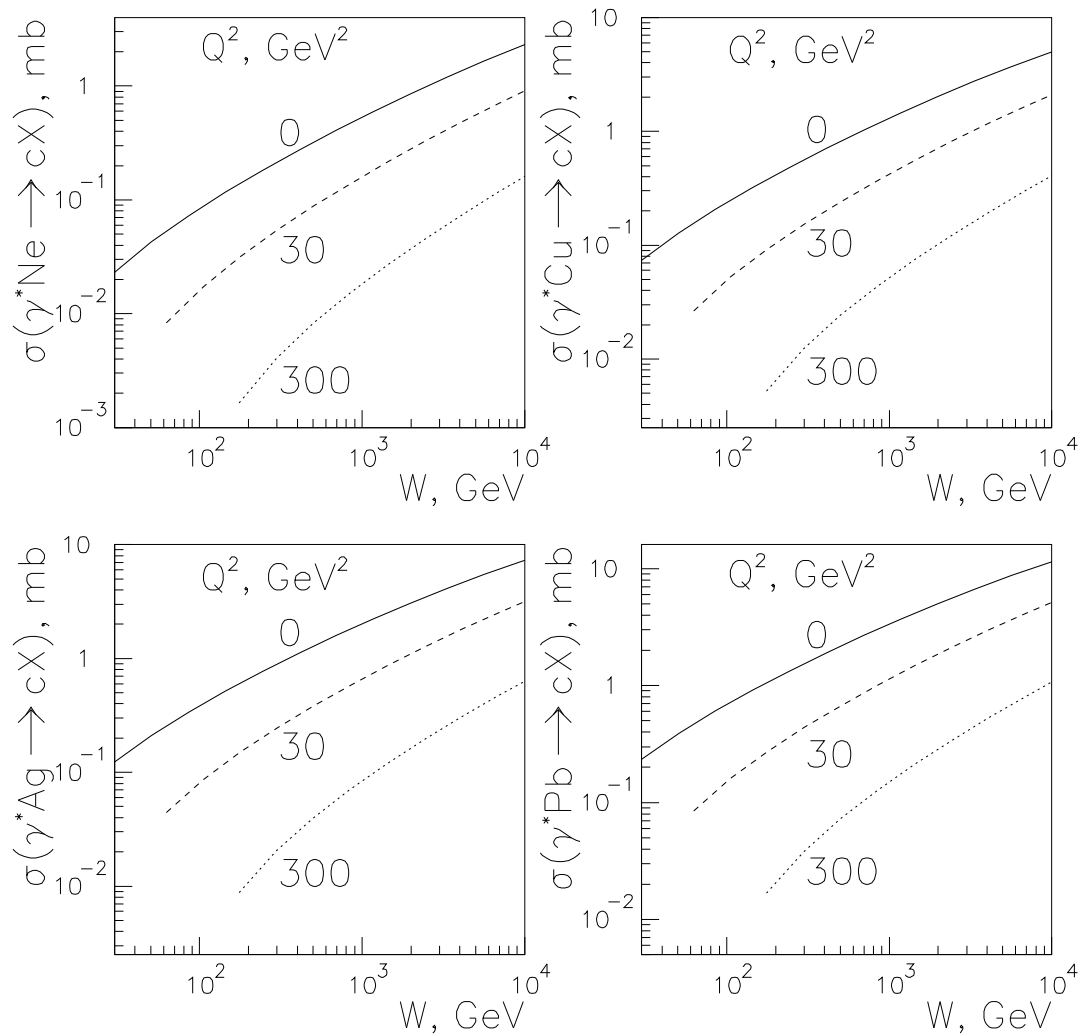


Figure 3:

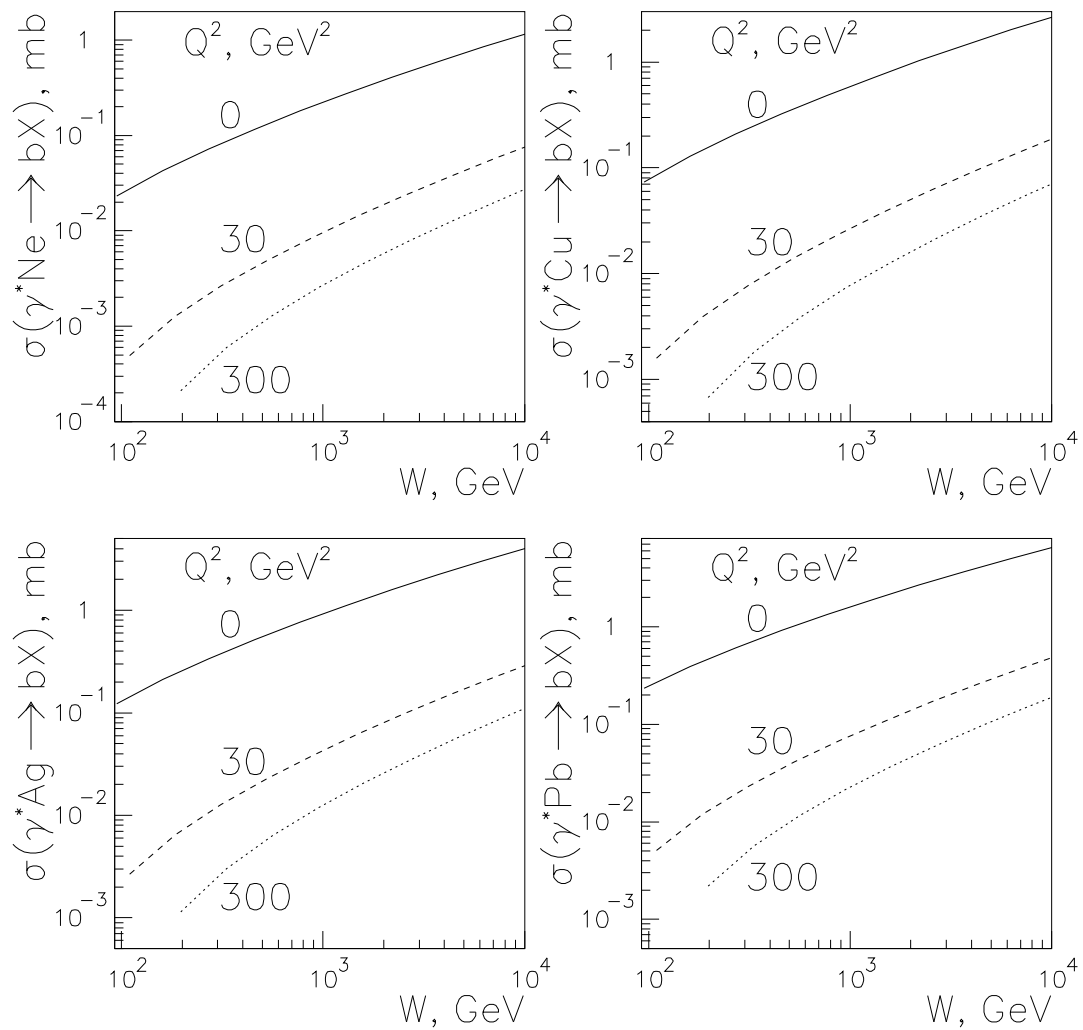


Figure 4:

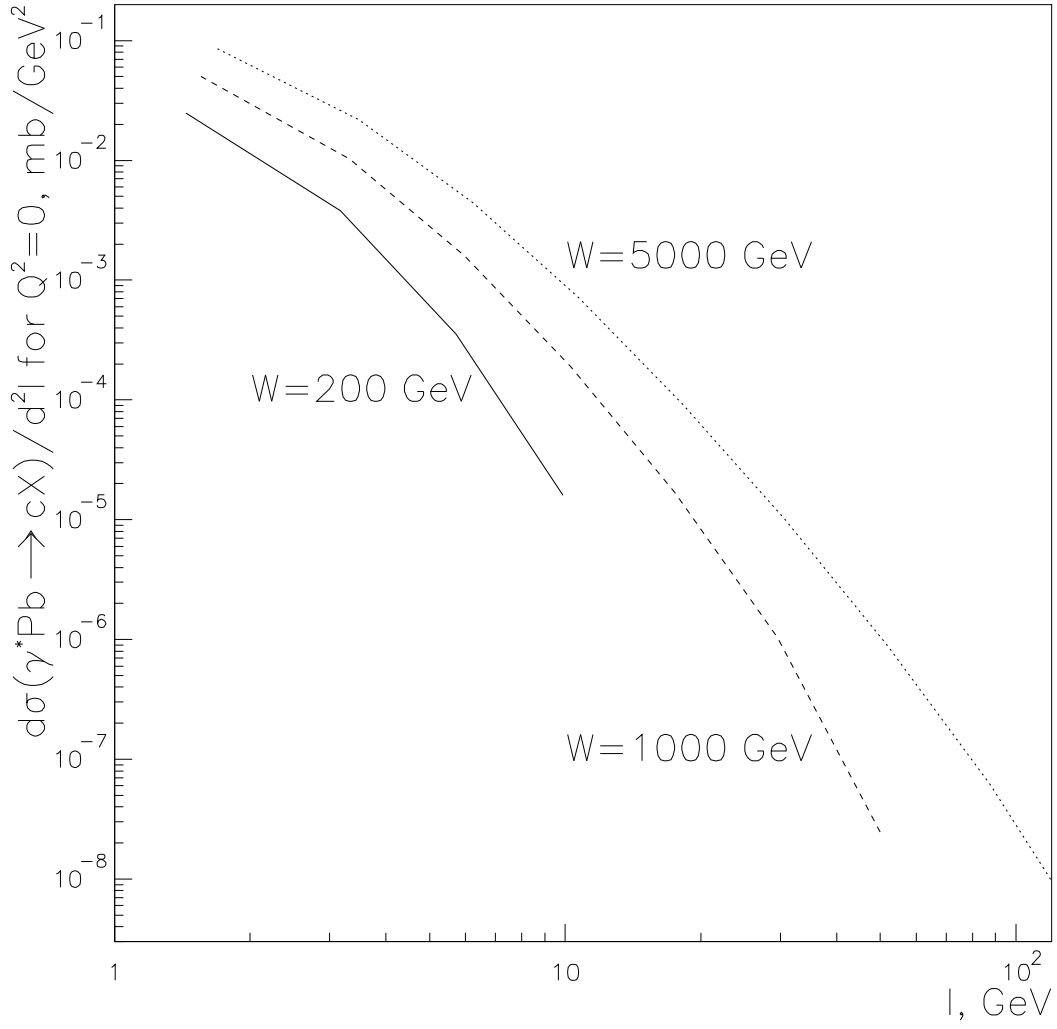


Figure 5:

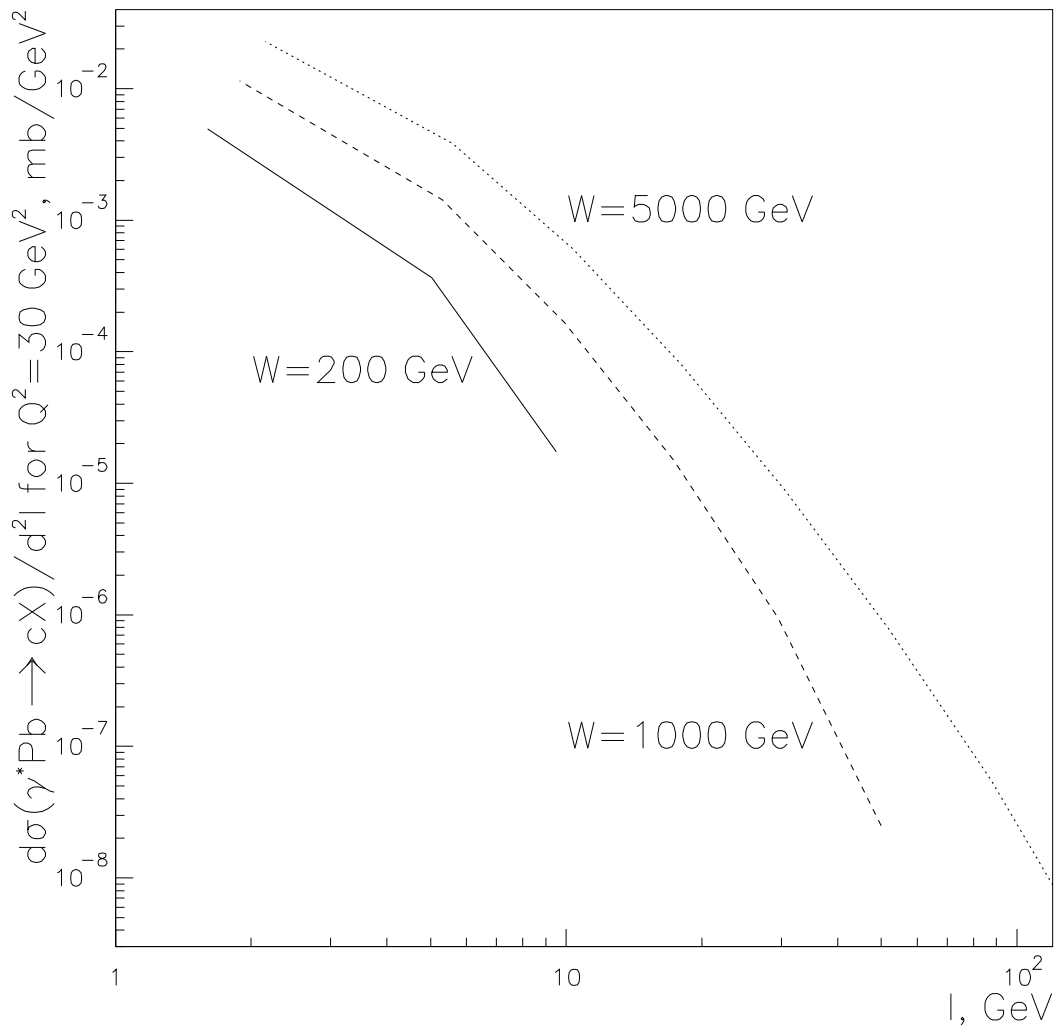


Figure 6: